

Batch-Fabricated Magnetic Sensors in Magnetic Foil Printed Circuit Board Technology

Martin A. M. Gijs and Eric Belloy

Institute of Microsystems, Swiss Federal Institute of Technology Lausanne,
CH-1015 Lausanne EPFL, Switzerland

(Received February 14, 2000; accepted October 16, 2000)

Key words: Planar transformer, fluxgate sensor, inductance, current sensor, PCB technology, flex-foil technology, amorphous magnetic foil, Vitrovac[®], Metglas[®]

We have combined micropatterned high-permeability ($\mu_r \sim 10^5$) amorphous magnetic ribbons with classical printed circuit board techniques to realise various types of inductive devices. We have used this batch technology to fabricate inductance and transformer devices in the 1–10 μH inductance range, as well as magnetic field and current sensors. These sensors are of the fluxgate type and are characterised by a sensitivity of 60 V/T at 30 kHz for the magnetic induction sensing devices, while for the current sensors we typically find sensitivities of 10 mV/A. We discuss our technology relative to other approaches in miniaturisation of magnetic devices.

1. Introduction

A low-cost and batch-fabricated magnetic sensor is interesting for many magnetic field and current sensing applications. A sensor of the inductive type is a good candidate for measuring small fields precisely and is, for this application, superior to magnetoresistive or Hall sensors. Therefore, inductive devices are at the heart of numerous precision measuring systems. With the increasing trend toward miniaturisation of electronic devices, often the inductive components are the determining factor limiting further size reduction. At the same time, an economically feasible component should be producible in a batch-like way and at low cost. Both for the realisation of high inductance transformers^(1–5) and for high-resolution magnetic sensing devices based on inductive measurement

principles like fluxgate sensors,⁽⁶⁻¹²⁾ the availability of a high-permeability and low-hysteresis ferromagnetic core material is essential.

We have developed a method for the fabrication of planar microtransformers,⁽¹³⁾ fluxgate magnetic induction⁽¹⁴⁾ and current⁽¹⁵⁾ sensing devices using a cheap printed circuit board (PCB)/amorphous magnetic foil technology, in which we integrate Cu winding patterns with patterned magnetic foil core materials. The magnetic core materials used (Vitrovac® 6025 or Metglas® 2714A) have an extremely high relative magnetic permeability ($\mu_r \sim 100\,000$) and are fairly thick (15–25 μm).^(16,17) This permeability is one or two orders of magnitude larger than the value for films made using classical vacuum deposition methods. Consequently, for a given inductor size, the value of the inductance can be much higher than that obtainable with those methods. For magnetic induction and current sensing devices, the sensor's response is proportional to the relative permeability of the core material; hence, a high μ_r is also beneficial here. Moreover, in our technology, the core material can be selected from a variety of commercially available amorphous magnetic foils amenable to lithographic patterning. Recently, such amorphous materials as well as others were used for the realisation of magnetic fluxgate sensors integrated with complementary metal oxide semiconductor (CMOS) circuitry.⁽¹⁸⁻²⁰⁾

In this paper, we report the fabrication method for our devices and subsequently discuss their applications as inductors, as sensitive magnetic field fluxgate sensors or as current sensors. First, we discuss microtransformers, which are composed of three functional layers, the outer of which carries the printed coil patterns; the inner is the Vitrovac® 6025 high-permeability ferromagnetic sheet core. Both magnetic metal and copper layers are patterned using standard lithographic techniques. In between the magnetic metal and copper layers there is a foil of solid epoxy glue for insulation and assembly. Connection between the outer copper patterns is realised by electroplating to complete the windings. These transformers are about 600 μm thick with lateral dimensions of approximately 1 cm and inductance values in the 10 μH range. Fluxgate magnetic field sensors are the second type of devices. The principle of a fluxgate is based on the external magnetic field-dependent periodic saturation of the ferromagnetic core. The combined action of the external field (to be measured) and excitation coils, driving the ferromagnetic core periodically in saturation, leads to the generation of higher order harmonics of the fundamental excitation frequency in a detection coil surrounding the magnetic core. The second harmonic voltage V_{2f} can be filtered out of the detection signal using a lock-in technique and is proportional to the external field for a given field range (typically 0.01–100 μT). Finally, we introduce current sensing as a third application of our technology. To realise a current sensor, we provide the magnetic fluxgate-type sensors with a hole in the centre of the PCB structure to accommodate a current-carrying wire. It is the magnetic field generated by the current through this wire which generates a second harmonic voltage over the excitation coil to which we apply an ac excitation current at frequencies of several tens of kHz. We have also measured the variation in response of our sensors due to their angular position with respect to the earth's magnetic field.

2. Fabrication Procedure

A schematic diagram of the coil fabrication process is shown in Fig 1. The proposed method of fabrication is very similar to a conventional PCB process. The devices are based on two epoxy boards (100 μm thick) with copper (35 μm thick) laminated on one side, and by a simple epoxy board (100 μm thick) as a support for the Vitrovac[®] 6025 magnetic foil in the case of the inductors and transformers; for the current sensors, we used Metglas[®] 2714A foils because of their superior etching characteristics. A liquid epoxy was used to laminate the magnetic foil to the inner epoxy board. Two 100- μm -thick sheets of Prepreg[®] solid epoxy were used for bonding the laminates into a stack of five layers.

The Vitrovac[®] and Metglas[®] foils were patterned photolithographically by first laminating sheets of solid negative photoresist (Ordyl[®] 200) onto degreased foils and then processing according to manufacturer's specifications after pattern transfer. A wet chemical process was developed in-house to etch the magnetic foils, consisting of exposure of the resist-covered Vitrovac[®] foils to a freshly prepared aqua regia etching bath ($\text{HNO}_3:\text{HCl}:\text{H}_2\text{O}$, 2:1:3) for several minutes at room temperature without agitation. For the Metglas[®] foils, we used a FeCl_3 solution. The photoresist proved itself immune to the etchant and exhibited excellent adhesion if the substrates were well cleaned. Figure 2 is a photograph of a patterned Metglas[®] magnetic foil glued on the inner epoxy board,

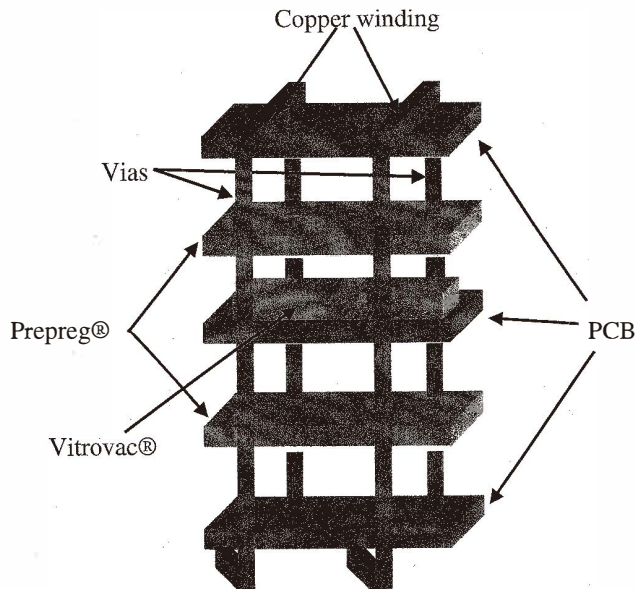


Fig. 1. Schematic diagram of our batch-type inductive magnetic device fabrication process.

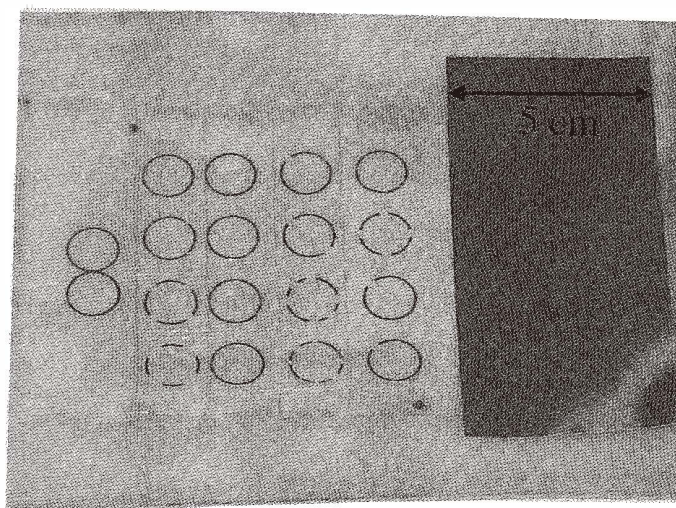


Fig. 2. Photograph of a patterned Metglas[®] magnetic foil on an epoxy board showing circular structures for current sensing applications; on the right, one observes the unpatterned foil material before it is glued onto the epoxy board.

showing circular structures for current sensing applications; on the right of the figure, one sees the raw unpatterned foil material before it is glued onto the epoxy board.

To align the PCB boards, a pinning system was used. The precision of the pin alignment holes defines the maximum lateral precision available with this technology (currently about $100\ \mu\text{m}$). Bonding operations were carried out by hot pressing typically at 180°C and $20\ \text{kg}/\text{cm}^2$. During the bonding step, the Prepreg[®] sheets melt, whereby the viscous liquid spreads out and contacts all interior surfaces under the applied pressure. Via holes were drilled at appropriate positions for the interconnects, which were subsequently metallised using copper electroplating. Winding patterns were produced on the outer copper layers photolithographically, thereby completing the helical coil pattern which fully encircles the interior magnetic core.

3. Experimental Results and Discussion

3.1 Inductors and transformers

Figure 3(a) shows the layout of the design of two rectangular transformers characterised by a primary set of windings (2×5 windings at the outer parts of the structure) and a set of 5 secondary windings at the central part of the structure. The Vitrovac[®] magnetic core is represented in grey and has a central part 2 mm wide, around which all windings are applied, and two side parts 1 mm wide for flux closure. These side parts of the magnetic core contain air gaps of variable width ($0\text{--}1000\ \mu\text{m}$) for tuning the effective permeability

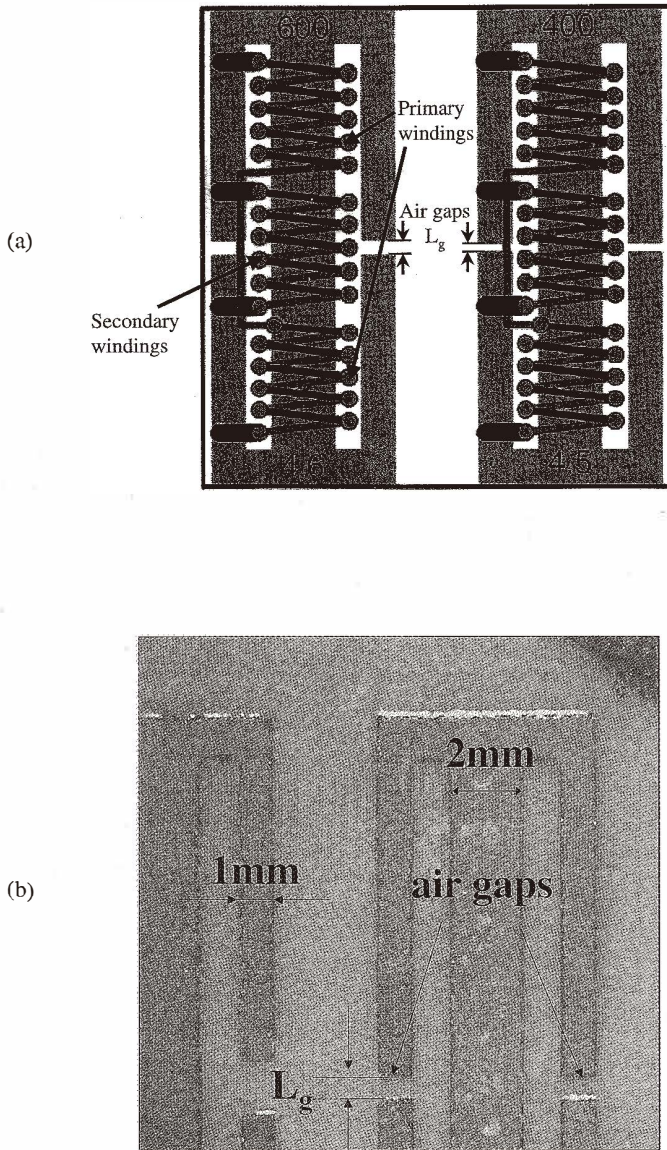


Fig. 3. (a) Design of two rectangular transformers showing the primary and secondary windings and the micropatterned magnetic material with air gaps. (b) Photograph of Vitrovac micropatterned magnetic foil cores.

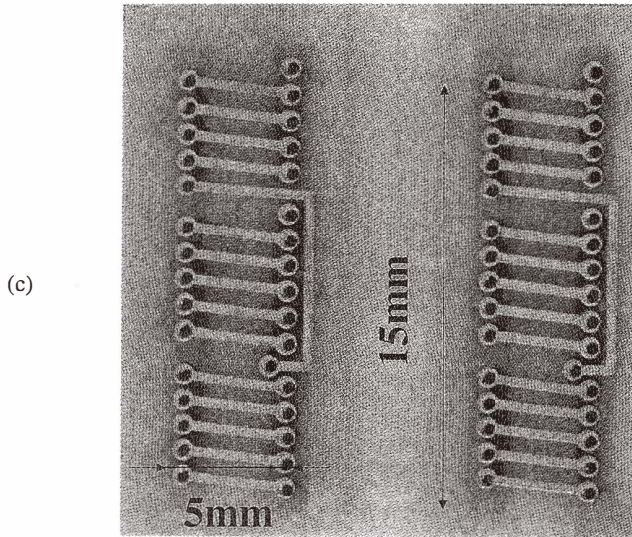


Fig. 3(c). (continued) Photograph of as-fabricated transformers.

and, hence, the inductance of the device. A photograph of the micropatterned magnetic core with air gaps L_g is shown in Fig. 3(b). Figure 3(c) is a photograph of two finalised devices showing the primary and secondary windings and the Cu interconnection holes.

The transformers and inductors have been electrically characterised using an HP4194A impedance/gain phase analyser. Inductance and resistance values are recorded simultaneously as a function of a logarithmic frequency sweep from 100 Hz up to 40 MHz using sinusoidal excitation signal levels of 100 and 500 mV rms. As an example, we show in Fig. 4 the frequency dependence of the primary self-inductance, L , and the coil resistance, R , measured on a 10-turn primary transformer with an open secondary winding and without a gap in the magnetic core. The self-inductance L attains its highest values at low frequencies, and in this case a maximum of about $3.5 \mu\text{H}$ is measured at 1 kHz. The inductance mainly follows the intrinsic permeability dependence of the Vitrovac® 6025 material. The rise in coil resistance starting at about 50 kHz is due to eddy current and magnetic core losses.

Figure 5 is a typical gain ($V_{\text{sec}}/V_{\text{prim}}$) plot for a transformer based on a circle-shaped magnetic core without a gap characterised by 18 primary windings and 5 secondary windings. The plot of the gain measures the real voltage transformation ratio and is indicative of the microtransformers' performance over a wide frequency range. In Fig. 5, the gain for a transformer in step-down configuration is plotted. This graph reveals a flat response of -12 dB starting at about 20 kHz and extending to about 1 MHz. This dB level corresponds to a voltage ratio of 0.25. Taking into account the turn ratio of 18:5, one ideally expects a voltage transformation of 0.28. The reduced gain at low frequencies is due to the relatively high ohmic resistance with respect to the inductance of the device, which limits the primary voltage available for transformation; at higher frequencies, the

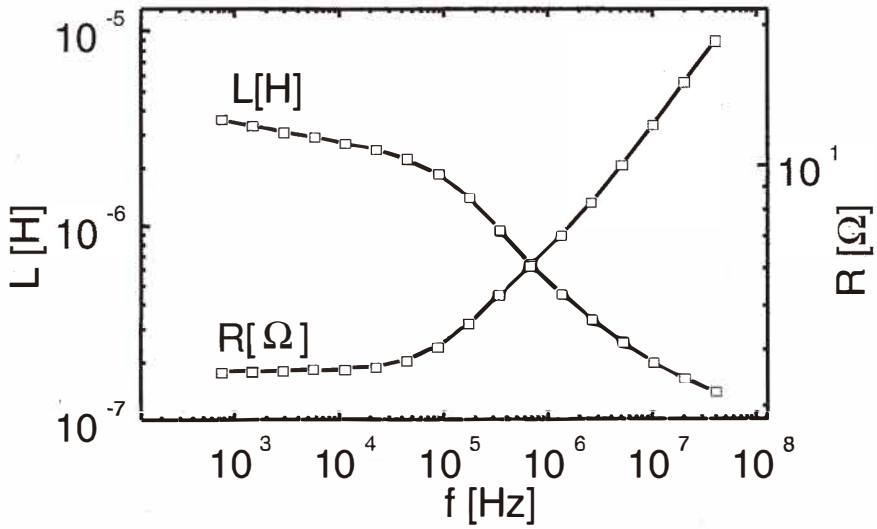


Fig. 4. Inductance and resistance as a function of frequency for a rectangular transformer without a gap.

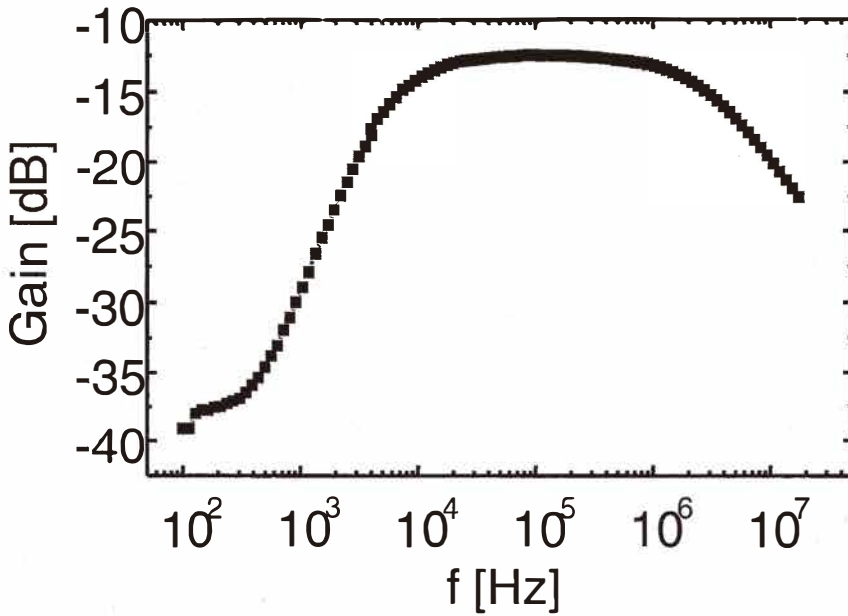


Fig. 5. Dependence of transformation gain on frequency for a microtransformer with a toroidal core shape.

inductive part of the impedance becomes dominant. At frequencies above 1 MHz, the intrinsic permeability of the magnetic material drops, which again decreases the inductive part of the impedance.

The effect of introducing air gaps in the outer legs of rectangular E-core-type transformers is demonstrated in Fig. 6 (curve a). The inductance L falls as the gap increases, thus behaving in a manner analogous to that of conventional transformers. However, L maintains a rather constant value after the gap reaches 0.2 mm. We discuss now that this is a phenomenon very specific to the two-dimensional design of our transformers. To a first approximation, the dependence of L on gap width L_g is given by:

$$L = \mu_0 N^2 A_c / (L_g + L_m / \mu_r), \quad (1)$$

where μ_0 is the permeability of free space, A_c is the cross-sectional area of the inner core leg, and L_m is the path length in the magnetic material. The other symbols have their usual meanings. This equation is plotted as curve b in Fig. 6, based on an effective μ_r of 16000, and L_m of 33.1 mm. However, the experimental values are grossly underestimated by this theoretical curve, which predicts a more rapid fall-off of L than is observed. Flux fringing around the gap, an effect which becomes more evident as the gap grows larger, can decrease the overall reluctance of the magnetic circuit, thereby offsetting the effect of the

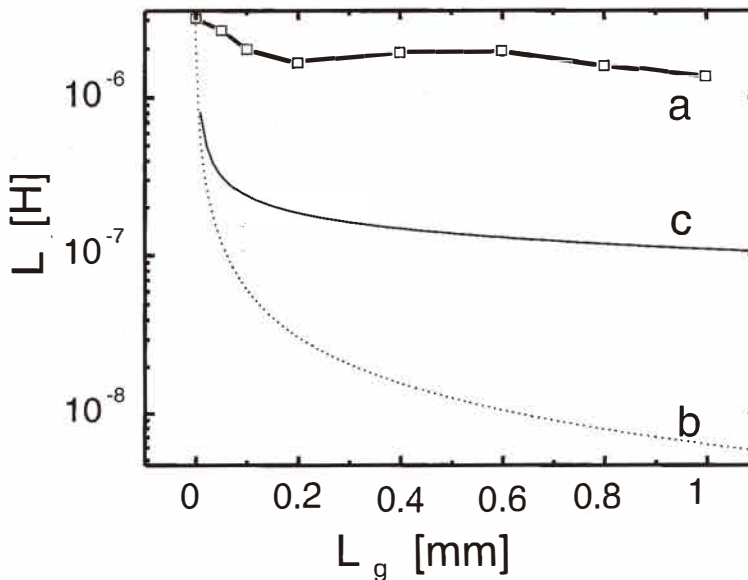


Fig. 6. Primary main inductance vs air gap at 1 kHz for transformers with rectangular magnetic core and $N = 10$: (a) measured value; (b) calculated value without fringe correction factor; and (c) calculated value including fringe correction.

increasing gap. This effect is not taken into account by eq. (1), but it can be estimated quantitatively by introducing a multiplicative correction factor F into eq. (1), where $F = 1 + L_g/A_c^{1/2} \ln(2G/L_g)$.^(21,22) G is the vertical dimension of the core window ($G = 14$ mm in our case).

We have plotted eq. (1) with the correction as curve c in Fig. 6, demonstrating that there is better agreement with the experimental data. Thus, classical fringing flux at least partially accounts for the observed behavior. We believe that the remaining difference between the theoretical value and the experiment is due to the two-dimensional character of the magnetic cores we use. Indeed, one can imagine and calculate numerically that flux fringing in a direction normal to the flat magnetic core will be relatively more important than in the parallel direction, and that hence the (simple) multiplication factor F does not accurately describe flux-fringing effects for our devices.

As an application of the inductors and transformer-type devices, one can think of embedded inductances on a PCB; using simple winding technology, one can easily obtain inductances of 10 μH or higher. One should note that due to the high relative permeability of the magnetic materials, these can saturate easily. However, by micropatterning them or by choosing foils with a lower permeability, one can avoid saturation up to reasonable current levels. On the other hand, for true power applications and for high frequencies, we think that inductors and transformers will be based on highly resistive ferrite-type materials.

3.2 Fluxgate magnetic field sensors

The layout of a fluxgate sensor in which the magnetic core material has been patterned into a rectangular shape is shown in Fig. 7(a). The two excitation coils have been grouped into four clusters of five windings and are symmetrically positioned around the inner five detection coil windings. Moreover, we have introduced air gaps in the magnetic core to tune the magnetic permeability and, hence, the sensitivity of the device. A series of rectangular fluxgate devices with gap lengths L_g varying between 0 and 1 mm were fabricated to investigate their influence on the sensitivity and the linear range of the magnetic sensor. A photograph of the experimental realisation of this fluxgate sensor is displayed in Fig. 7(b).

For experimental characterisation, the excitation coils were fed with an ac excitation current of 100–500 mA_{p-p} provided by an HP 6825A bipolar power supply at frequencies of 10–30 kHz. The fluxgate response to an external magnetic field B_{ext} was monitored by connecting the detection coil to an EG&G 7260 lock-in amplifier tuned to the second harmonic frequency $2f$. Computer-controlled measurements of the second harmonic voltage V_{2f} were made as a function of the external field B_{ext} generated by Helmholtz coils placed symmetrically around the fluxgate device. These coils were fed with a dc current provided by a programmable Keithley 2400 power supply.

Figure 8 represents the second harmonic voltage V_{2f} of the detection coil of a rectangular fluxgate sensor as a function of B_{ext} for various gap lengths L_g at a frequency of 10 kHz and for an excitation current of 300 mA_{p-p}. The field B_{ext} is applied in-plane

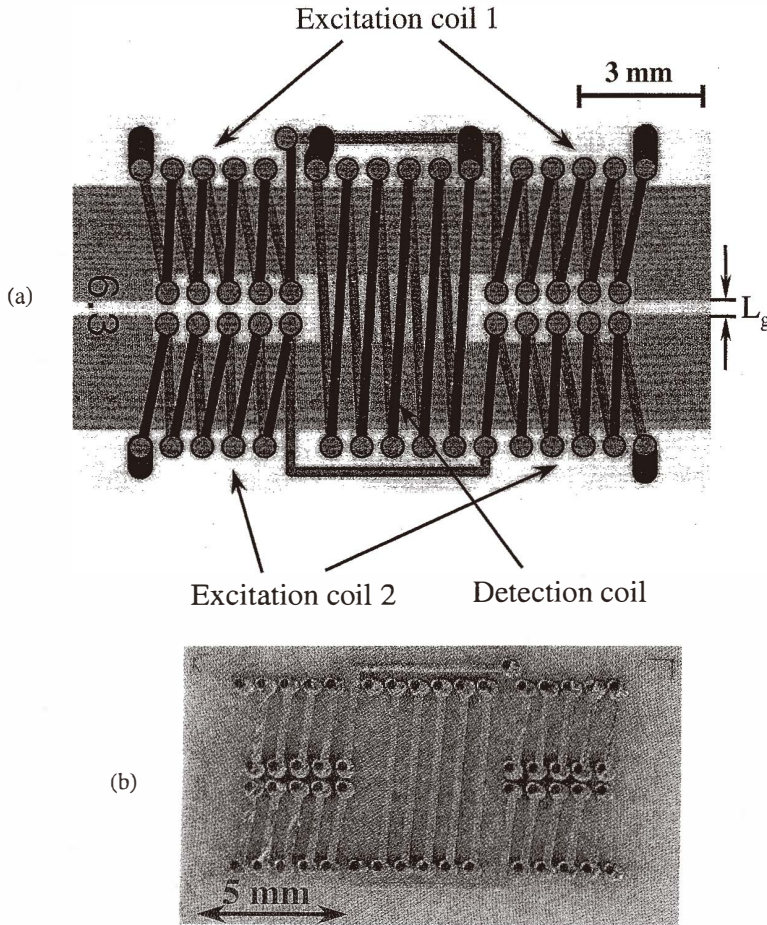


Fig. 7. (a) Schematic diagram of a rectangular fluxgate sensor showing the primary and secondary windings and the micropatterned magnetic material with air gaps L_g . (b) Photograph of as-fabricated rectangular fluxgate sensor.

perpendicular to the detection coil as shown schematically in the insert of Fig. 8. The three curves are characterised by a linear slope at low B_{ext} . For $L_g = 0$ mm, one notes a maximum field, limiting this linear range of $B_{lin,max} \approx 110 \mu T$, while the maximum value of V_{2f} is around $280 \mu T$. For $L_g = 0.5$ mm and 1 mm the maxima of the linear ranges $B_{lin,max}$ are shifted to higher B_{ext} , while the maximum of the curves is found at the same external field $B_{ext} = 280 \mu T$ in both cases. In other words, the slopes of the linear parts of the $V_{2f} - B_{ext}$ curves decrease with increasing gap length L_g . This graph clearly shows that, by choosing a certain air gap L_g , one can select the fluxgate sensor's sensitivity and the linear

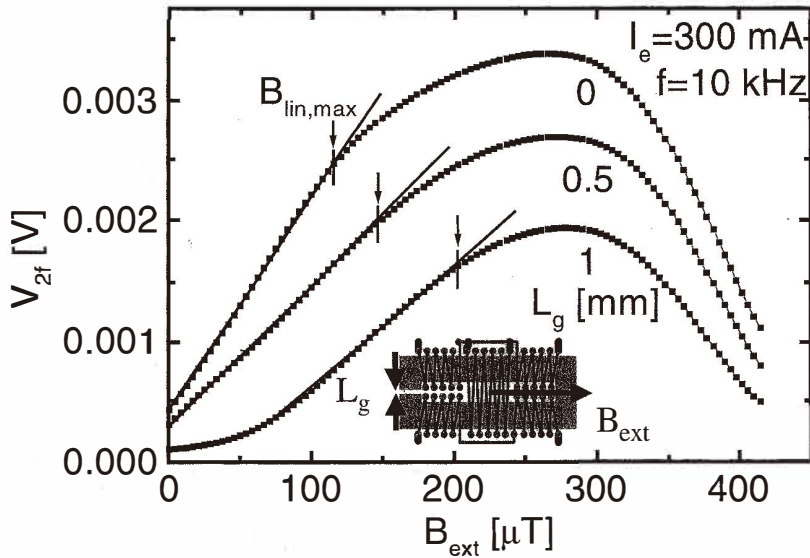


Fig. 8. Second harmonic voltage V_{2f} of the detection coil of a rectangular fluxgate sensor as a function of the external field B_{ext} for various gap lengths L_g using an excitation current of 300 mA at 10 kHz.

magnetic field regime. The magnetic field sensitivity $S_b = \frac{dV_{2f}}{dB_{ext}}$ in the linear field range of this fluxgate sensor ranges between 0.01 and 0.02 mV/μT. By increasing the number of windings of our devices, we have obtained sensitivities on the order of 60 V/T. Kawahito *et al.*⁽⁹⁾ have shown that, upon excitation of the fluxgate sensor by an ac magnetic field with triangular waveform, the Fourier analysis of the induced voltage in the detection coil gives rise to a second harmonic voltage V_{2f} given by:

$$V_{2f} = \frac{8NA\mu_r^*B_m f}{\pi} \sin \frac{\pi \Delta B}{B_m} \sin \frac{\pi B_{ext}}{B_m}, \quad (2)$$

where N is the number of turns of the detection coil, A is the cross-section of the area of the core, μ_r^* is the effective relative permeability and B_m the maximum magnetic induction generated by the excitation current. The term $\Delta B = 2B_s / \mu_r^*$ (B_s is the saturation magnetic induction). Under the optimal excitation condition where the peak excitation field is twice the saturation field, Kawahito *et al.* start from eq. (2) and derive a magnetic sensitivity of the fluxgate sensor

$$S_B[V/T] = dV_{2f}/dB_{ext} = 8NA\mu_r^*f. \quad (3)$$

Equation (3) clearly shows the linear dependence on the various characteristic parameters of the fluxgate sensor, in particular the influence of the effective relative permeability μ_r^* that decreases with increasing air gap length L_g .

Figure 9 represents the amplitude of the voltage V_{2f} of the second harmonic of the detection coil of a rectangular fluxgate sensor without an air gap in the Vitrovac® magnetic material as a function of the external magnetic induction B_{ext} for various excitation currents I_e at 10 kHz. We have chosen the direction of B_{ext} along the line of the horizontal component of the local terrestrial magnetic field ($\approx 20 \mu\text{T}$). One notes that for all excitation currents, V_{2f} approaches zero in this field; this situation corresponds to an effective zero magnetic field. For all I_e , there is also a linear dependence on B_{ext} in the low-field range. This range becomes more extended for the higher excitation currents. The symmetric response around the true zero field with respect to the sign of the external magnetic field is immediately clear. Moreover, the curves shown in Fig. 9 represent data taken by increasing the external field from $-250 \mu\text{T}$ up to $250 \mu\text{T}$ and vice versa. Within the limit of our detection, we found no evidence of hysteresis (which should be smaller than $0.5 \mu\text{T}$).

It is interesting to compare the properties and performance of our fluxgate sensors with the published work of Chiesi *et al.*,⁽¹⁸⁾ Kawahito *et al.*,⁽¹⁹⁾ and Schneider⁽²⁰⁾ (see Table 1).

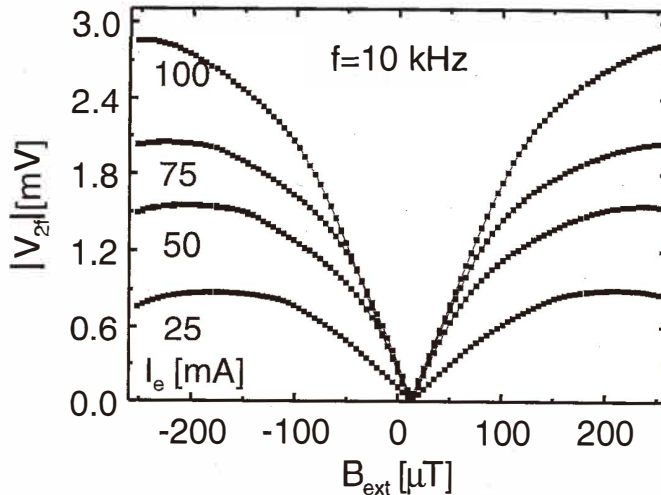


Fig. 9. Second harmonic voltage V_{2f} (plotted as the absolute value) of the detection coil of a rectangular fluxgate sensor without an air gap ($L_g = 0 \text{ mm}$) as a function of B_{ext} for various excitation currents I_e at 10 kHz.

While we realise a 'bare' fluxgate device in the PCB material, the two other approaches integrate very small fluxgate sensing devices directly on a Si substrate containing a CMOS driver and detection electronics. Moreover, the design of the magnetic core and the electrical winding patterns have been chosen somewhat differently from ours. From table 1, it is clear that the size of the Si integrated devices is much smaller. We and researchers in ref. (18) use for the magnetic core an amorphous magnetic alloy with extremely high permeability at frequencies below 100 kHz, while the devices of refs. (19) and (20) are based on an electroplated NiFeMo alloy, which has an appreciable permeability, and are also used at higher frequencies. It is clear from eq. (3) that both effective permeability of the magnetic material core and frequency are important for having a high sensitivity.

Excitation currents are for all devices of the order of 20 up to 200 mA and the number of windings in the excitation coil(s) N_{exc} is of the same order. For the detection coil, our devices have a smaller number of electrical windings N_{det} , compared to the other two approaches; this is related to the resolution of the used PCB, rather than Si technology. The best results in terms of sensitivity and power dissipation are found for the device of Chiesi *et al.* One can say that nonlinear and hysteretic effects for the three types of devices are comparable and small. The angular resolution of the two integrated devices, when used as a compass, is of the order of a few degree.

Table 1

Comparison of the characteristics and performance of our PCB-based fluxgate sensor with published results of two types of fluxgate devices integrated 'on-chip.'

Ref.	This study	Chiesi <i>et al.</i> ⁽¹⁸⁾	Kawahito <i>et al.</i> , ⁽¹⁹⁾ and Schneider ⁽²⁰⁾
Type	Sensor only	Sensor + chip	Sensor + chip
Size	1 cm × 1 cm	5.3 mm ²	5.6 mm × 3.4 mm
Magnetic mat.	Vitrovac [®]	Metglas [®]	NiFeMo
Intrinsic permeab.	10 ⁵ –10 ⁶	10 ⁵ –10 ⁶	3000–20 000
Effective permeab.	10 ⁴	1400	2200–7000
Excitation current	50–250 mA	17 mA	45 mA
N_{exc}	20	40	18
Excit. frequency	10–30 kHz	125 kHz	2.5 MHz
Power dissipation	30–500 mW	12.5 mW	325 mW
N_{det}	5	4 × 50	2 × 41
Sensitivity	60 V/T	180 V/T	21 V/T
Sensit. after amplif.	–	3760 V/T	–
Linear regime	± 150 μT	± 100 μT	± 50 μT
Nonlinearity	–	–	1.5 μT for B < 50 μT
Hysteresis	< 0.5 μT	2 μT at B = 400 μT	–
Angular resolution	–	1.5°	4°
Noise	–	–	6 nT/Hz ^{1/2}

From the application point of view, we think that our device is useful for those applications where extreme miniaturisation is not an issue. In that case, one can directly mount and bond an application-specific-integrated-circuit (ASIC) on the PCB containing the fluxgate sensor. No special postprocessing of magnetic materials on the Si wafer is necessary. When the dimensions of the device are critical and miniaturisation is required for the application, one will choose for an integrated device.

3.3 Current sensors

Our technology can be used equally well for the realisation of current sensors; in this case, we measure the magnetic field generated by a dc current through a wire which is inserted inside a hole at the central point of the sensor. Figure 10(a) is a photograph of the layout of one type of device. It consists of two excitation coils consisting of 18 windings each centred around a PCB embedded ring patterned out of Metglas® 2714. This patterned core can be simple, as shown in Fig. 10(a), or can contain 'gaps' to diminish sensitivity and to extend the current measuring range of the device. For the measurement of a dc current, we apply an ac excitation current to the two coils in series and measure the amplitude of the voltage of the second harmonic over the same coils. Clearly, a higher dc current introduces a larger asymmetry in the saturation characteristics of the magnetic material and a larger second harmonic component. The central coil, consisting of four windings, is the analogue of the detection coil for the fluxgate magnetic field measurements and is not used for the current sensing experiments. Figure 10(b) is a photograph of the actual realisation of the current sensing device.

A typical current measurement is shown in Fig. 11 for a sensor having a gap-free magnetic core. We present here the second harmonic voltage amplitude V_{2f} vs dc current I_{DC} through a wire placed within the hole in the sensor. One observes curves measured at three different excitation frequencies with a rms amplitude of 175 mA. We observe a similar characteristic as with the magnetic field fluxgate measurements, i.e., a linear-like zone at small I_{DC} , hence a small field, followed by a maximum and subsequently a decrease in the sensor's response. With increased frequency, the sensor output is also enhanced. The measured sensitivity of the sensor is about 10 mV/A. The sensor will have a maximum response when the absolute value of the magnetic field induced by the ac current is on the order of the magnetic field of the dc current to be measured.

To have an idea of the immunity of the current sensor to an external magnetic field, we show in Fig. 12 the second harmonic voltage amplitude V_{2f} as a function of the positioning of another device with respect to the earth's magnetic field. This sensor is characterised by four gaps of 3 mm each patterned in the ferromagnetic material. This gives a reduced effective permeability and hence a reduced sensitivity of the device, typically 0.2–0.3 mV/A. The excitation current in Fig. 12 is at 30 kHz with a rms current value of 350 mA. The position of the sensor at 0° corresponds to the symmetry axis of the sensor aligned with the direction of the earth's magnetic field. The understanding of this field dependence is rather complicated and involves both asymmetry induced by the electrical winding patterns and asymmetry induced by the micropatterning of the four gaps in the magnetic material. A more detailed study of these influences on the orientational dependence of the current sensors is the subject of future research.

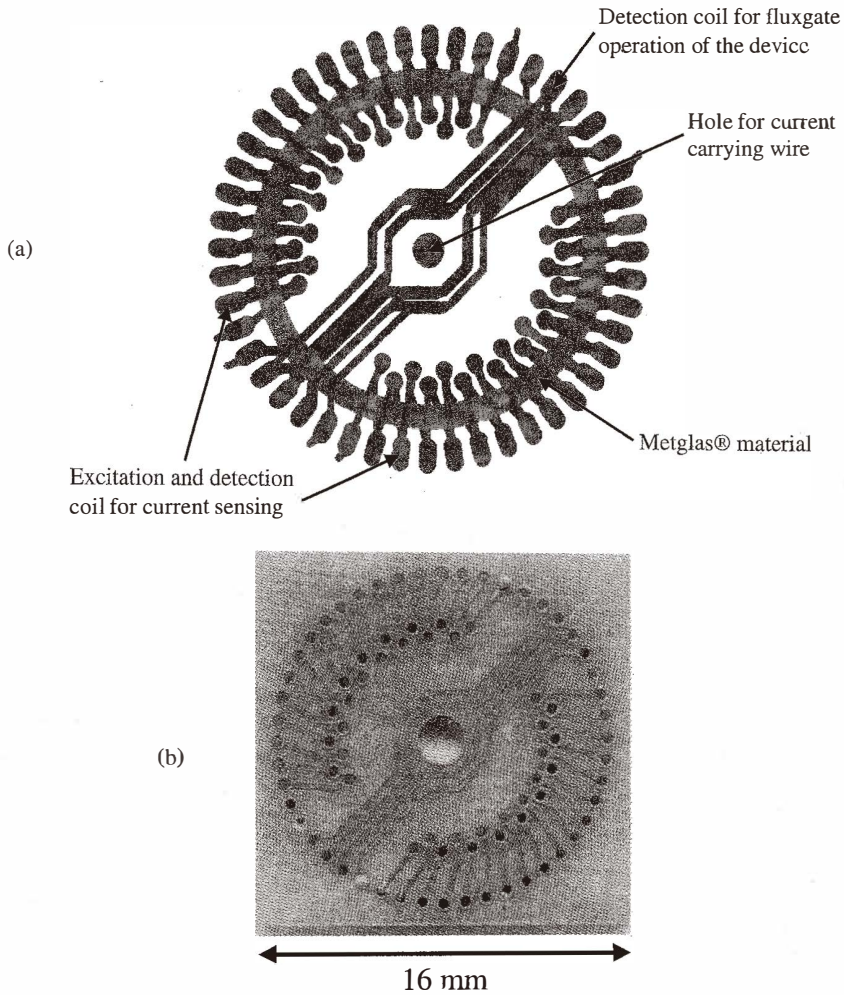


Fig. 10. (a) Schematic diagram of a toroidal current sensor showing the windings of the excitation/detection coils, the micropatterned magnetic material and the access hole for the current carrying wire. (b) Photograph of a realised current sensor.

To finalise the discussion of our results, we can say we have demonstrated the feasibility of the PCB technology in which we have integrated an ultrahigh permeability magnetic foil in the PCB stack. From a technological point of view, this does not drastically change PCB manufacturing procedures, as one is used to working with Cu foils and, for the Metglas®, one uses similar etchants as for patterning Cu. Therefore, we think that from an industrial point of view our technology will be quite competitive, as the typical cost will be on the order of the cost of conventional PCB technology.

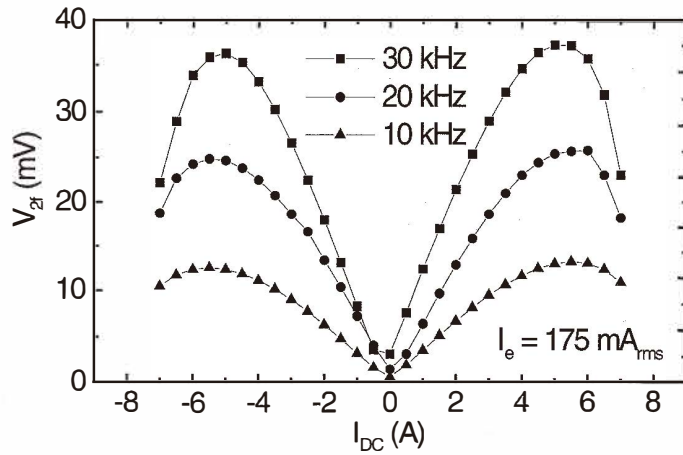


Fig. 11. Second harmonic voltage V_{2f} as a function of applied dc current for a sensor with a complete magnetic core and using an excitation current $I_e = 175 \text{ mA}_{\text{rms}}$ at three different excitation frequencies.

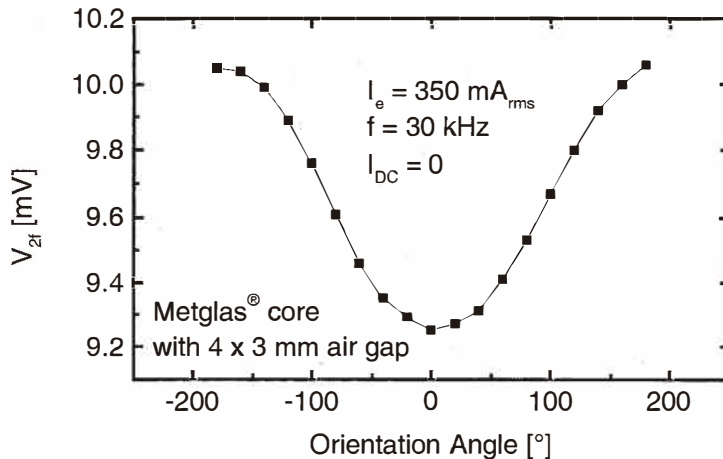


Fig. 12. Second harmonic voltage V_{2f} as a function of orientation angle of the sensor with respect to the earth's magnetic field for a sensor with a magnetic core containing four gaps of 3 mm using an excitation current $I_e = 350 \text{ mA}_{\text{rms}}$ at 30 kHz.

We have presented three types of devices based on this technology: inductors and transformers, fluxgate magnetic induction sensors and current sensors. We think that fluxgate magnetic induction sensors are very attractive devices for realisation with our technology. We can benefit from and combine the design freedom of photolithography, the ultrahigh permeability of the magnetic material at an appreciable foil thickness and the

economic aspects of PCB technology. Moreover, a fluxgate magnetic induction sensor can be easily integrated with its electronics by simply bonding an ASIC onto the PCB.

The same holds for current sensing; the high magnetic field sensitivity can be exploited for the measurement of dc and low-frequency ac currents. As for the fluxgate magnetic induction sensor, we can simply tune its sensitivity by changing the shape of the micropatterned magnetic core, the frequency or simply the number of windings.

4. Conclusions

In this paper, we have presented a batch technology based on a low-cost PCB process. The use of an amorphous metal foil as a magnetic core permits the facile development of high-performance inductive devices: inductances of 1–10 μH at 1 kHz for the transformers and a sensitivity of up to 60 V/T at 30 kHz for the fluxgates. For the applications as current sensors, we report sensitivities of typically 10 mV/A. In comparison with other technologies, our devices are larger than the fully integrated ones; however, our process avoids time-consuming and expensive thin-film post-processing on the Si wafer, while retaining compatibility with standard electronic packaging schemes. Therefore, our technology opens the way to a new class of functional and economic sensing devices for applications where extreme miniaturisation is not an issue.

Acknowledgements

The authors thank O. Dezuari and S. Gilbert for their contributions at the initial stage of the work and M. Hermanjat and Ph. Vossler for their help and advice in PCB processing.

References

- 1 J. Y. Park, L. K. Lagorce and M. G. Allen: IEEE Trans. Magn. **33** (1997) 3322.
- 2 B. Löchel, A. Maciossek, M. Rothe and W. Windbracke: Sensors and Actuators A **54** (1996) 663.
- 3 M. Mino, T. Yachi, A. Tago, K. Yanagisawa and K. Sakakibara: IEEE Trans. Magn. **28** (1992) 1969.
- 4 K. Yamasawa, K. Maruyama, I. Hirohama and P. P. Biringer: IEEE Trans. Mag. **26** (1990) 1204.
- 5 H. Tsujimoto and T. Koiso: IEEE Trans. Magn. **32** (1996) 4980.
- 6 F. Primdahl: J. Phys. E: Sci. Instrum. **12** (1979) 241.
- 7 P. Ripka: Sensors and Actuators A **33** (1992) 129.
- 8 N. Pollock: Wireless World (1982) 49.
- 9 S. Kawahito, Y. Sasaki, H. Sato, T. Nakamura and Y. Tadokoro: Sensors and Actuators A **43** (1994) 128.
- 10 T. Seitz: Sensors and Actuators A **21–23** (1990) 799.
- 11 S. O. Choi, S. Kawahito, Y. Matsumoto, M. Ishida and Y. Tadokoro: Sensors and Actuators A **55** (1996) 121.
- 12 R. Gottfried-Gottfried, W. Budde, R. Jähne, H. Kück, B. Sauer, S. Ulbricht and U. Wende: Sensors and Actuators A **54** (1996) 443.

- 13 O. Dezuari, S. E. Gilbert, E. Belloy and M. A. M. Gijs: *Sensors and Actuators A* **71** (1998) 198.
- 14 O. Dezuari, E. Belloy, S. E. Gilbert and M. A. M. Gijs: *IEEE Trans. Magn.* **35** (1999) 2111.
- 15 E. Belloy, S. E. Gilbert, O. Dezuari, M. Sancho and M. A. M. Gijs: *Sensors and Actuators A* **85** (2000).
- 16 R. Boll: *Soft Magnetic Materials* (Vacuumschmelze GmbH, Hanau, 1993).
- 17 Metglas® product literature (AlliedSignal, Morristown, NJ, USA 1998).
- 18 L. Chiesi, P. Kejik, B. Janossy and R. S. Popovic: *Sensors and Actuators A* **82** (2000) 174.
- 19 S. Kawahito, C. Maier, M. Schneider, M. Zimmermann and H. Baltes: *IEEE J. of Solid-State Circuits* **34** (1999) 1843.
- 20 M. Schneider: *CMOS Magnetotransistor and Fluxgate Vector Sensors*, Ph.D thesis no. 12746 ETH Zürich (1999).
- 21 W. T. McLyman: *Transformer and Inductor Design Handbook*, 2nd ed. (Marcel Dekker, New York, 1988) p. 50.
- 22 R. Lee, L. Wilson and C. E. Carter: *Electronic Transformers and Circuits*, 3rd ed. (John Wiley & Sons, New York, 1988).

Eric Belloy was born in Geneva, Switzerland in 1972. He received his diploma in Microengineering in 1997 from the Swiss Federal Institute of Technology of Lausanne (EPFL). His diploma work was the study, realisation and characterisation of microtips on Si and glass substrates for the detection of the electrical activity of nerve cells. Since April 1997, he has been working as a research assistant at the Institute of Microsystems at EPFL and is developing a new technology based on flex-foil patterning and assembling to realise magnetic devices. He is also involved in the development of three-dimensional microfabrication processes using powder blasting.

Martin A. M. Gijs received his degree in Physics in 1981 from the Katholieke Universiteit Leuven, Belgium and his Ph.D. degree in Physics at the same university in 1986. He joined the Philips Research Laboratories in Eindhoven, The Netherlands in 1987. Subsequently, he has worked there on micro- and nanofabrication processes of high critical temperature superconducting Josephson and tunnel junctions, the microfabrication of microstructures in magnetic multilayers showing the giant magnetoresistance effect, the design and realisation of miniaturised motors for hard disk applications and the design and realisation of planar transformers for miniaturised power applications. He joined the Swiss Federal Institute of Technology of Lausanne (Ecole Polytechnique Fédérale de Lausanne) in 1997 as a professor in the Institute of Microsystems of the Microengineering Department, where he is responsible for the Microsystems Technology group. His main interests are in developing technologies for novel inductive-type devices, new microfabrication technologies for the fabrication of microsystems in general and the development and use of microsystems technologies for biomedical applications in particular.